NANO LETTERS

pubs.acs.org/NanoLett

Letter

Cesium Copper Halide Perovskite Nanocrystal-Based Photon-Managing Devices for Enhanced Ultraviolet Photon Harvesting

Junyu Wang, Tong Cai, and Ou Chen*

Cite This: *Nano Lett.* 2023, 23, 4367−4374

Read Online

ACCESS | Metrics & More | Article Recommendations | Supporting Information

ABSTRACT: Space-based solar power harvesting systems with high levels of specific power (the power produced per mass of the mounted photovoltaic cell) are highly desired. In this study, we synthesized high quality lead-free $Cs_3Cu_2Cl_5$ perovskite nanodisks with efficient ultraviolet (UV) photon absorption, high photoluminescence quantum yields, and a large Stokes shift, which are suitable to serve as photon energy downshifting emitters in the applications of photon-managing devices especially for space solar power harvesting. To demonstrate this possibility, we have fabricated two types of photon-managing devices, i.e., luminescent solar concentrators (LSCs) and luminescent downshifting (LDS) layers. Both experimental results and simulation analyses show that the fabricated LSC and LDS devices exhibit high visible light transmission, low photon scattering and reabsorption energy loss, high UV photon harvesting, and energy conversion after integrating with silicon-based photovoltaic cells. Our research presents a new avenue for utilizing lead-free perovskite nanomaterials in space applications.

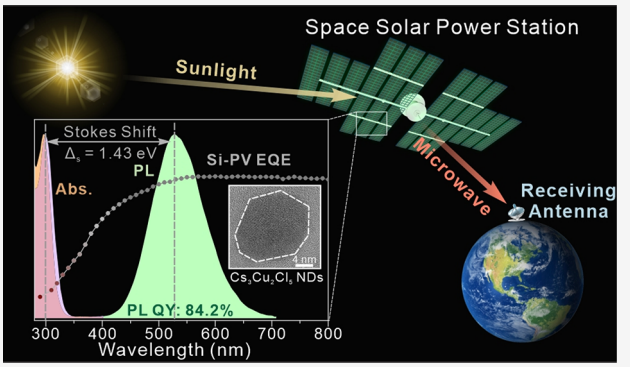

KEYWORDS: *lead-free perovskites, copper halide perovskite nanocrystals, luminescent solar concentrators, luminescent downshifting layers, space solar energy*

Ever since the discovery of crystalline silicon wafer in the early 1950s, researchers have been considering integrating photovoltaic (PV) systems with aerospace satellites to harvest solar energies in space.[1−5] With this idea in mind, researchers have recently proposed a space-based solar power system that is composed of a spacecraft carrying an array of utility-scale PVs into geostationary orbit for efficient solar energy harvesting in space (Scheme 1).[6−8] The generated electricity can be radiated through an antenna system mounted on the spacecraft and collected by the receiving stations placed on earth (Scheme 1).[8−10] Practically, the solar harvesting system needs to reach a high level of specific power (defined as the power produced per mass of the mounted PV cell, unit of kW/kg) for sufficient solar photon to electricity conversion.[7] Theoretically, the space-based solar panels can generate 2000 GW of power constantly, which is ∼40 times more energy than on earth due to the continuous generation of electricity under direct solar irradiance.[11−14] However, for the standalone PV system, it is difficult to exceed a specific power of 1 kW/kg,[15] which is the minimal requirement for a solar energy generation station.[7] This is mainly due to the dimension limitation of the mounted PV cells and their low efficiency for the high-energy UV photon collection and conversion.[6,7,16] In particular, the solar radiation in space consists of ∼7% UV light of the total solar spectrum, i.e., 0.45% UVC (100−280 nm), 1.12% UVB (280−315 nm), and 5.43% UVA (315−400 nm) photons, which is ∼2.5 times more than the total UV radiation on the earth's surface (due to the strong UV absorption and scattering effects by the ozone layer).[17,18] Therefore, desirable lightweight photon-managing devices are pressingly needed to boost the specific power, especially by more efficiently harvesting high-energy UV photons through aerospace satellite systems. In this regard, luminescent solar concentrator (LSC) is a dielectric device that can harvest, direct, and concentrate incoming photons to small areas for the use of energy conversion by the attached PV cells.[19−24] And the luminescent downshifting (LDS) layer can be directly attached to PV top surface to improve the short-wavelength response of PV modules by downconverting high-energy photons to a longer wavelength range.[25−29] The integration of LSC or LDS devices has been proposed as a potential solution for boosting the solar energy harvesting and increasing the specific power of space-based solar panels.[16,30−32]

Received: February 17, 2023
Revised: April 28, 2023
Published: May 4, 2023

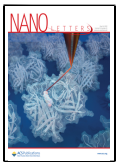

Scheme 1. Schematic Demonstration for the Working Principle of Space-Based Solar Power Station Integrated with Either LSC-PV or LDS-PV Device Systems

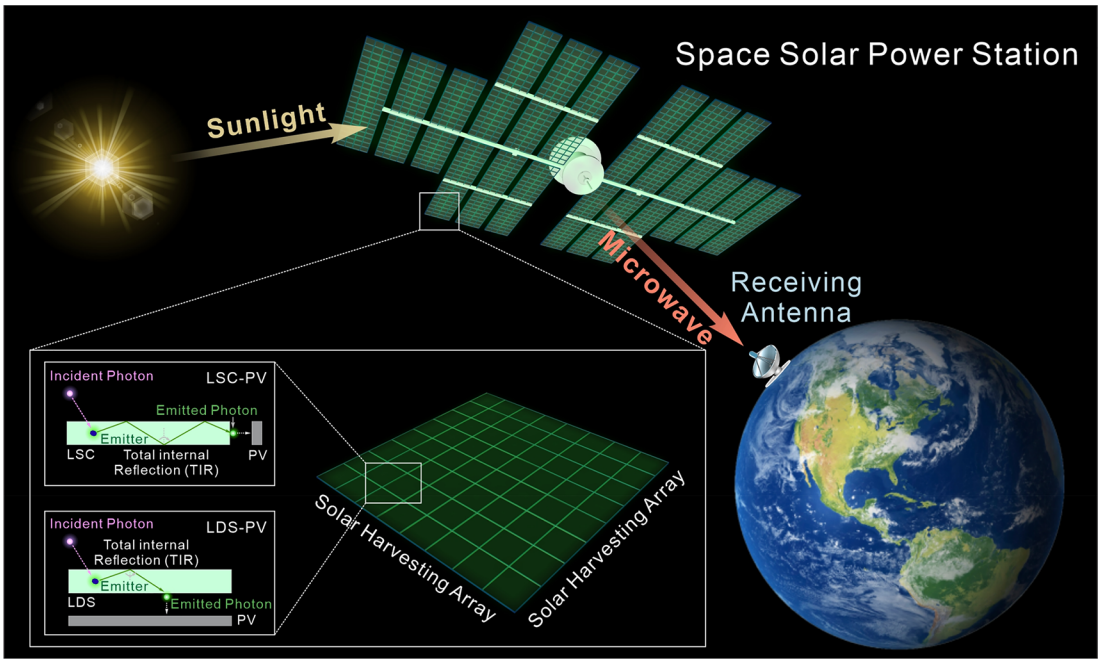

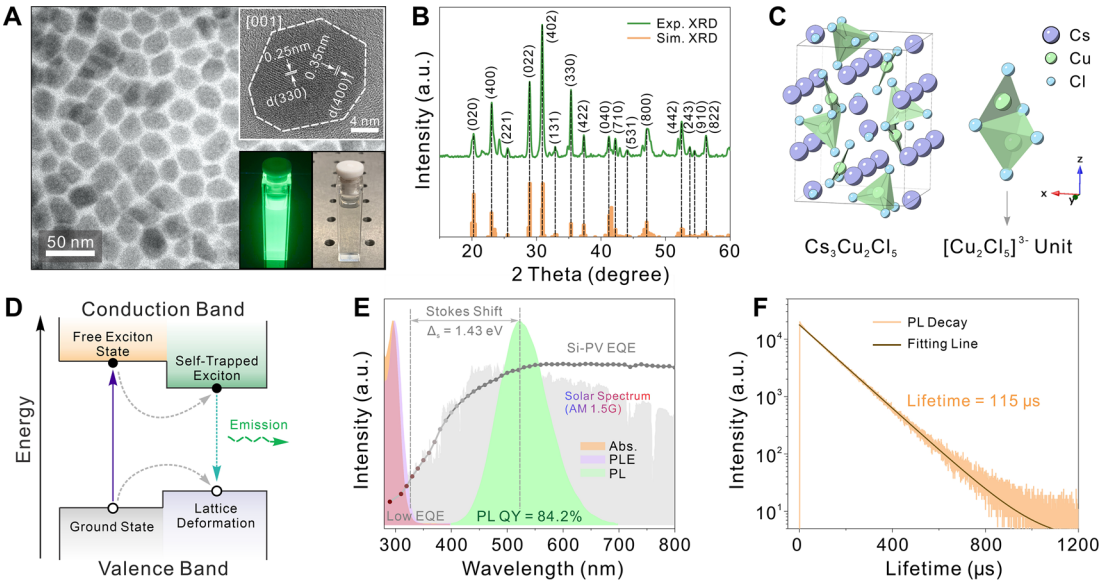

Figure 1. (A) Typical TEM image of the $Cs_3Cu_2Cl_5$ NDs. Inset: HR-TEM image of one representative $Cs_3Cu_2Cl_5$ ND (top); photographs of $Cs_3Cu_2Cl_5$ NDs hexane solution under UV light illumination and room light (bottom). (B) Experimental (Exp.) and simulated (Sim.) XRD patterns of the $Cs_3Cu_2Cl_5$ NDs. (C) Unit cell structure and a $[Cu_2Cl_5]^{3-}$ unit of $Cs_3Cu_2Cl_5$ NDs. (D) Band structure alignment of $Cs_3Cu_2Cl_5$ perovskite. (E) Absorption (Abs.), photoluminescence excitation (PLE), and photoluminescence (PL) spectra of the $Cs_3Cu_2Cl_5$ NDs along with a standard calibrated external quantum efficiency (EQE) plot (gray) of silicon−photovoltaic cell (Si-PV). Gray shade represents the solar radiation spectrum with AM = 1.5. (F) Time-resolved PL decay curve and fitting line of the $Cs_3Cu_2Cl_5$ NDs in a hexane solution.

Halide perovskite nanocrystals (NCs) are promising emitters for LSC and LDS layer integrations due to their tunable optical bandgap, narrow emission peak, and high photoluminescent quantum yield (PL QY).[16,33−37] In particular, a new family of lead-free copper(I)-based metal halide (i.e., $Cs_3Cu_2X_5$, X = Cl, Br, and I) perovskite NCs has recently been synthesized with multiple merits, i.e., strong UV photon absorption, high transparency in visible spectral region, green/blue emissions with high PL QYs (>80%), and a large Stokes shift with a non-reabsorption feature, making them ideal for LSC and LDS integrations in PV cells, especially for space-based solar panels.[38−40] However, to our best knowledge, the copper(I)-based metal halide perovskite NCs have not yet been demonstrated in LSC or LDS device applications.

Herein, we synthesized lead-free $Cs_3Cu_2Cl_5$ perovskite nanodisks (NDs) with a high PL QY of 84.2% and a large Stokes shift of 1.43 eV. By incorporating these NDs into LSC and LDS devices using an ultrasonic spray coating method, we achieved high visible light transmission, low photon scattering, and superior UV photon harvesting and energy conversion

https://doi.org/10.1021/acs.nanolett.3c00641
Nano Lett. 2023, 23, 4367−4374

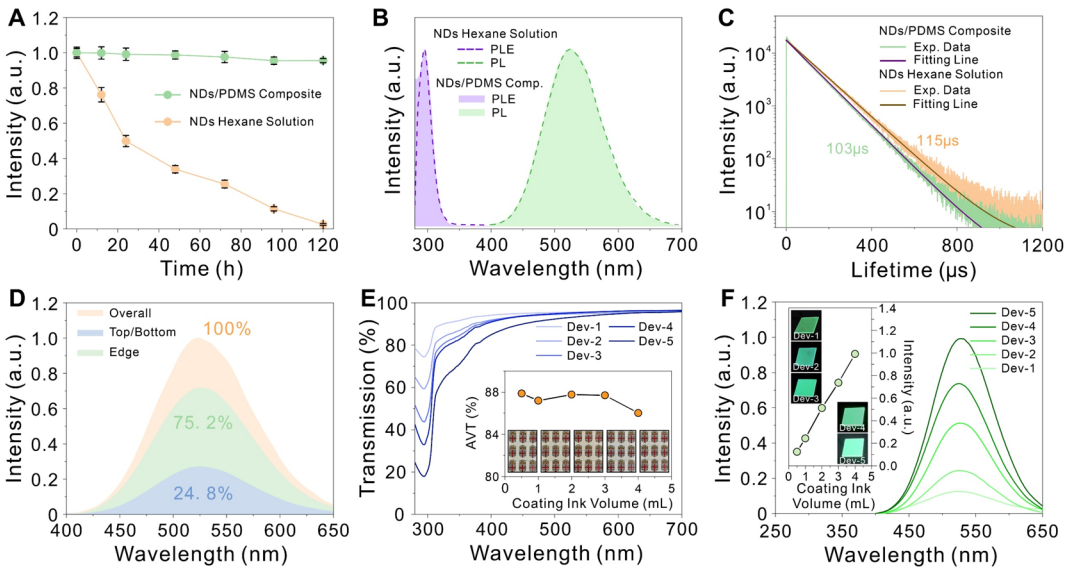

Figure 2. (A) Normalized PL intensity evolutions of a $Cs_3Cu_2Cl_5$ NDs hexane solution and a $Cs_3Cu_2Cl_5$ NDs/PDMS composite device as a function of time under ambient conditions. (B) Photoluminescence excitation (PLE) and photoluminescence (PL) spectra of $Cs_3Cu_2Cl_5$ NDs hexane solution and $Cs_3Cu_2Cl_5$ NDs/PDMS composite device. (C) Time-resolved PL decay curves of a NDs/PDMS composite device and a NDs hexane solution. (D) PL spectra collected from the top/bottom surfaces, the edge, and the total $Cs_3Cu_2Cl_5$ NDs/PDMS composite device (the device dimension of 4.0 cm × 4.0 cm × 0.1 cm). (E) Transmission spectra of a series of $Cs_3Cu_2Cl_5$ NDs/PDMS composite devices with different coating volume of NDs ink solution. Inset: the corresponding average visible transmittance (AVT) and photographs (under ambient light) of the $Cs_3Cu_2Cl_5$ NDs/PDMS devices. (F) PL spectra with relative intensity of the series of $Cs_3Cu_2Cl_5$ NDs/PDMS devices. Inset: the PL peak intensity and photographs (under UV light) of the corresponding devices coated with different volumes of NDs ink solution.

when integrated with Si-PV cells. A maximum of over 30-fold (6-fold) enhancement can be obtained for the LSC (LDS) devices for UV photon utilization when comparing their applications in space and on earth. Our results demonstrate the potential of using these unique photon-managing devices as spacecraft photon collection portholes or as multifunctional energy collection hulls with increased specific power. This study opens a new door for applying lead-free perovskite nanomaterials to enhance high-energy photon utilization in space-based solar power systems.

Colloidal lead-free $Cs_3Cu_2Cl_5$ perovskite NDs were synthesized following a literature method.[41,42] Briefly, oleylamine hydrochloride precursor was injected into 1-octadecene solution containing cupric acetate, cesium carbonate, and oleic acid at 120 °C to initiate the particle formation reaction. Transmission electron microscopy (TEM) measurements showed that the average lateral size of the as-prepared $Cs_3Cu_2Cl_5$ NDs is 20.7 ± 3.1 nm (Figures 1A and S1). A high-resolution TEM (HR-TEM) image of individual ND showed clear lattice fringes with a *d* spacing of 2.5 Å, which can be assigned to the interplanar distance of (330) planes in the orthorhombic phase of $Cs_3Cu_2Cl_5$ perovskite NDs (Figure 1A, inset).[38,41−43] The X-ray diffraction (XRD) pattern of the sample confirmed the orthorhombic crystal structure with all the major Bragg diffraction peaks assigned to the simulated $Cs_3Cu_2Cl_5$ perovskite peak positions (Figure 1B). The unit cell structure of $Cs_3Cu_2Cl_5$ perovskite is shown in Figure 1C, which adopts an orthorhombic structure in the space group of *Pnma* with isolated $[Cu_2Cl_5]^{3-}$ dimers.[39−42,44,45] Absorption and PL (under 295 nm light excitation) spectroscopic measurements revealed that the NDs showed a strong UVC and UVB absorbance with the first absorption peak at 294 nm, corresponding to the Cu *d*−*d* electronic transition.[41,43] Importantly, the sample exhibited a large Stokes shift of 1.43 eV with a strong self-trapping exciton (STE) emission peak centered at 524 nm (full width at half-maximum, FWHM: ∼470 meV) (Figure 1E). A high PL QY of the synthesized $Cs_3Cu_2Cl_5$ perovskite NDs was determined to be 84.2%. Time-resolved PL spectroscopy measurements (under 295 nm light excitation) revealed a PL decay lifetime of 115 μs (Figure 1F), in agreement with the STE emission characteristics as well as previously reported values.[41,45,46]

The obtained $Cs_3Cu_2Cl_5$ perovskite NDs were then used to fabricate LSC/LDS photon-managing devices using our recently developed ultrasonic spray-coating method (see fabrication details in the Supporting Information).[20] Briefly, an ink solution containing $Cs_3Cu_2Cl_5$ perovskite NDs, polydimethylsiloxane (PDMS), and hexane was sprayed onto a preheated PDMS substrate using an ultrasonic nebulizer. The ink solution contained 8.0 wt % NDs with respect to the PDMS, and the PDMS/hexane volume ratio was 1/10. The ultrasonic vibration generator produced micrometer-scale droplets from the ink solution, forming an even deposition onto the substrate. After hexane evaporation, the resulting NDs/PDMS composite was cured to form a transparent film. To enhance the device stability and protect the $Cs_3Cu_2Cl_5$ perovskite NDs from oxygen and moisture, a thin layer of PDMS (∼2.5 μm) was subsequently spray-coated onto the device. Because of its stability to UV radiation, low surface energy (−21 mJ/cm^2), and strong Si−O−Si (siloxane) backbone, PDMS can effectively protect the $Cs_3Cu_2Cl_5$ perovskite NDs from oxygen, moisture, and degradation caused by high-energy photons. A device stability test showed that after 7-day storage in the atmosphere, the emission intensity of the $Cs_3Cu_2Cl_5$ NDs/PDMS composite remained ∼96% of the initial value, as compared to only 2.5% remained for the $Cs_3Cu_2Cl_5$ NDs dispersed in a hexane solution (Figure 2A). Both PL and PLE spectra of the $Cs_3Cu_2Cl_5$ NDs

https://doi.org/10.1021/acs.nanolett.3c00641
Nano Lett. 2023, 23, 4367−4374

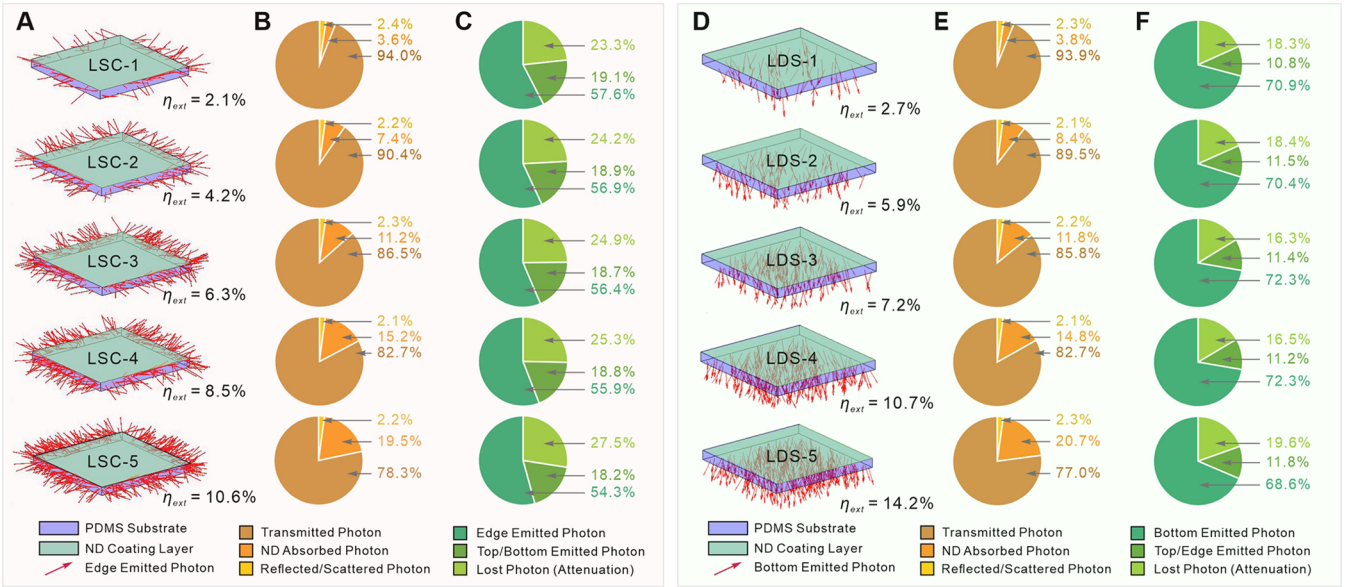

Figure 3. (A, D) Visualizations of the Monte Carlo ray-tracing simulation (MC simulation) for the $Cs_3Cu_2Cl_5$ NDs/PDMS composite devices serving as LSC (A) and LDS (D) devices. The arrows represent the photon output from the edge (bottom) regions of the LSC (LDS) devices. (B, E) Pie charts of incident photon fractions after hitting the surface of the LSC (B) and LDS (E) devices. (C, F) Pie charts of the fates of the absorbed photons for the LSC (C) and LDS (F) devices.

remained intact after being incorporated into the NDs/PDMS composite (Figure 2B). However, the PL lifetime was slightly shortened to 103 μs compared to that of a colloidal solution of the $Cs_3Cu_2Cl_5$ NDs (Figure 2C), indicating minimal non-radiative decay channels were introduced during the device fabrication process.[19,22] Due to the large Stokes shift with non-reabsorption behavior of the $Cs_3Cu_2Cl_5$ NDs, the emission light-trapping efficiency (defined as $\eta_{trap} = \sqrt{1 - n^{-2}}$, where n is the refractive index of the polymer matrix) of the NDs/PDMS composite was measured to be 75.2% (Figure 2D), in good accordance with the theoretically calculated value of 71.5% based on the refractive index of PDMS polymer (n = 1.43), indicating negligible photon scattering and attenuation losses.[20,23,47]

To tune the device performance, we then fabricated a series of NDs/PDMS composite devices by ultrasonic spray coating different volumes of the ND−ink solution with a constant $Cs_3Cu_2Cl_5$ NDs concentration of 8.0 wt % (with respect to the PDMS): 0.5 mL (Device-1), 1.0 mL (Device-2), 2.0 mL (Device-3), 3.0 mL (Device-4), and 4.0 mL (Device-5). With increasing the volume of coating ink solution while maintaining a low scattering effect, the devices showed a trend of decreasing (increasing) transmission (absorption) in the UV spectral range, which was attributed to the strong UV light absorption of the employed $Cs_3Cu_2Cl_5$ perovskite NDs (Figure 2E). Only a slight scattering effect can be visualized when the coating ink solution volume reached 4.0 mL (Figure 2E, Figures S2 and S3). Both the UV-only absorption behavior of the $Cs_3Cu_2Cl_5$ NDs and low light scattering of the NDs/PMDS composite devices warranted a high average visible transmittance (AVT) value of >85% for all the fabricated devices, demonstrating a superior visible transparency property (Figure 2E). The PL spectral profiles of all the devices showed a single emission peak centered at 527 nm (Figure 2F), in good accordance with the emission spectrum of the dilute NDs hexane solution (Figure 1E). Moreover, the PL peak intensity increased proportionally as increasing the coating volume (i.e., the amount of coated $Cs_3Cu_2Cl_5$ NDs) (Figure 2F), further confirming a negligible level of emitter aggregation in the fabricated devices.[20,48]

We used Monte Carlo (MC) ray-tracing simulation to evaluate the photon propagation performance of $Cs_3Cu_2Cl_5$ NDs/PDMS composite devices (see simulation details in the Supporting Information). The logic flows of the MC simulations for LSC and LDS devices are presented in Schemes S2 and S3. To achieve statistically significant simulation results, we set 12000 incident photons (wavelength of 305 nm) to hit the top surface of the devices (cuboid slab dimension: 4.0 cm × 4.0 cm × 0.1 cm; refractive index, n = 1.43, taken from the refractive index of PDMS). A $Cs_3Cu_2Cl_5$ NDs coating layer with a thickness of ∼2.5−20.0 μm was considered in the MC simulation. The experimentally measured device absorption spectra were used as the input absorption spectral profiles (Figure S4). We quantitatively traced incident photons after they hit the device top surface using the photon tracking counters in the MC model. For the MC simulations of LSC devices, when the coating volume increased from 0.5 to 4.0 mL, the edge-emitted photons increased from 2.1%, 4.2%, 6.3%, 8.5%, to 10.6% of the total incident photons (Figure 3A). Meanwhile, the transmitted (absorbed) photons gradually decreased (increased) from 94.0% to 78.3% (from 3.6% to 19.5%). And the fraction of the reflected and scattered photon loss was kept in a low range of 2.1−2.4% (Figure 3B), consistent with the experimental observations with minimal scattering signals (Figure 2E,F). The fates of ND-processed photons (absorbed and emitted photons by the NDs) were also analyzed and are shown in Figure 3C. While the fractions of escaped (through escape cone of top/bottom surfaces of the devices) and lost photons were maintained at similar levels of ∼19% and ∼25%, respectively, the collected photons from the edge windows of the devices remained a high fraction of ∼56%.

The MC ray-tracing simulation results for the LDS layers are shown in Figure 3D−F. The portion of collected photons at

https://doi.org/10.1021/acs.nanolett.3c00641
Nano Lett. 2023, 23, 4367−4374

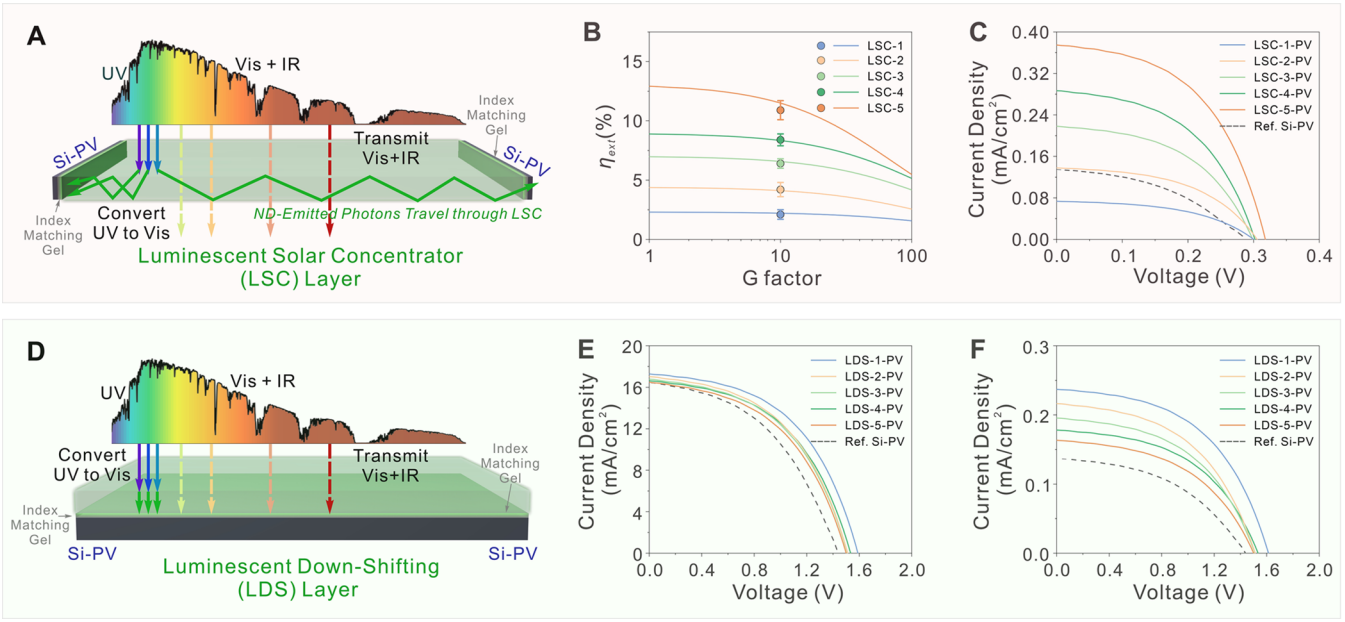

Figure 4. (A) Schematic demonstration of the working principle of an LSC device. (B) Experimental (spheres) and simulated (lines) η_{ext} for the $Cs_3Cu_2Cl_5$ NDs/PDMS composite LSC devices coated with different amounts of $Cs_3Cu_2Cl_5$ NDs coating ink solution. Evolutions of the η_{ext} as a function of G factor under 305 nm light excitation. (C) Experimentally measured $J-V$ curves of the LSC devices under 305 nm light excitation. (D) Schematic demonstration of the working principle of an LDS device. (E, F) Experimentally measured $J-V$ curves of the $Cs_3Cu_2Cl_5$ NDs/PDMS composite LDS devices coated with different amounts of $Cs_3Cu_2Cl_5$ NDs coating ink solution under solar simulator (E) and 305 nm light (F) excitations.

the bottom surface of the LDS devices increased from 2.7% to 14.2% as the coating volume increased from 0.5 to 4.0 mL (Figure 3D). The statistical result of the first photon contacting process of the LDS layers is similar to the result of the LSC devices. The transmitted (absorbed) photons decreased (increased) from 93.8% to 77.1% (from 3.8% to 20.7%) while increasing the amount of coated $Cs_3Cu_2Cl_5$ NDs (Figure 3E). At the same time, the statistical result for the fates of the photon behavior for LDS layers is shown in Figure 3F. For the emitted green photons downshifted by the $Cs_3Cu_2Cl_5$ NDs, the portion of the escaped photon (from the top and edge windows) maintained at a low level of ∼11%, and the fraction of lost photons (through attenuation) kept at ∼18% of the total downshifted photons. The bottom emitted photon kept at a higher level of ∼71%. The relatively low level of photon loss can be largely attributed to the reabsorption free characteristic of the $Cs_3Cu_2Cl_5$ NDs. Overall, the MC simulation combined with the experimental results revealed that the ND-based LSC and LDS devices exhibited a consistent and high light-trapping efficiency, suggesting a superior property of the $Cs_3Cu_2Cl_5$ perovskite NDs for UV light harvesting, downconverting, and trapping performance for the subsequent PV-based energy-conversion utilization.

Next, we performed electro-optical measurements to evaluate the performances of the $Cs_3Cu_2Cl_5$ NDs/PDMS devices used as either a LSC or a LDS layer to the attached Si−PV cells (Figure 4). The working principle of the LSC-PV device is shown in Figure 4A. The internal optical efficiency (η_{int}, the ratio of the edge-collected photon flux and the total absorbed photon flux) of the five LSC devices was measured to be 58.1% (LSC-1), 56.2% (LSC-2), 56.3% (LSC-3), 55.5% (LSC-4), and 54.1% (LSC-5) under 305 nm light illumination (Figure S5). The relatively stable η_{int} values across all the devices indicated minimal photon scattering and quenching effects, in good agreement with the device transmission/emission measurements (Figure 2E,F) and the MC simulation results (Figure 3A−C). We attributed the slight reduction in η_{int} to the scattering effect resulting from surface roughness. In contrast, the external optical efficiency (η_{ext}, the ratio of the edge-collected photon flux and the total incident photon flux) showed a continuous increase from 2.1 ± 0.4% (LSC-1), 4.2 ± 0.6% (LSC-2), 6.4 ± 0.4% (LSC-3), 8.4 ± 0.5% (LSC-4) to 10.9 ± 0.8% (LSC-5) (Figure 4B), in line with the MC simulation prediction as well as analytical mode simulation results (Figures 3A and 4B; see simulation details in the Supporting Information). In addition, we coupled commercial Si-PV cell onto the edge of the LSC devices and measured the current−density ($J-V$) plots for each LSC-PV construct as well as the standalone Si−PV as reference under 305 nm UV light illumination (see the measurement details in the Supporting Information). The short-current densities of the reference Si-PV and LSC-PV systems were obtained to be 0.135 mA/cm^2 (Si−PV), 0.074 mA/cm^2 (LSC-1-PV), 0.138 mA/cm^2 (LSC-2-PV), 0.218 mA/cm^2 (LSC-3-PV), 0.287 mA/cm^2 (LSC-4-PV), and 0.375 mA/cm^2 (LSC-5-PV) (Figure 4C). The external optical efficiency (η_{ext}) calculated based on the $J-V$ curve measurements was consistent with the values obtained from the optical measurements as well as the MC simulation (Figure S6). These results showed that the integrated LSC-PV systems can outperform the standalone Si-PV cell for UV light harvesting and conversion when enough $Cs_3Cu_2Cl_5$ NDs was incorporated to the LSC device.

To examine the possibility of applying $Cs_3Cu_2Cl_5$ perovskite NDs for LDS devices, we attached the NDs/PDMS films onto Si−PV cells to construct an LDS-PV system (Figure 4D). To minimize the total internal reflection, an index matching gel (refractive index of 1.52) was applied at the interface between NDs/PDMS LDS layer and Si−PV cell (Figure 4D). Under

https://doi.org/10.1021/acs.nanolett.3c00641
Nano Lett. 2023, 23, 4367−4374

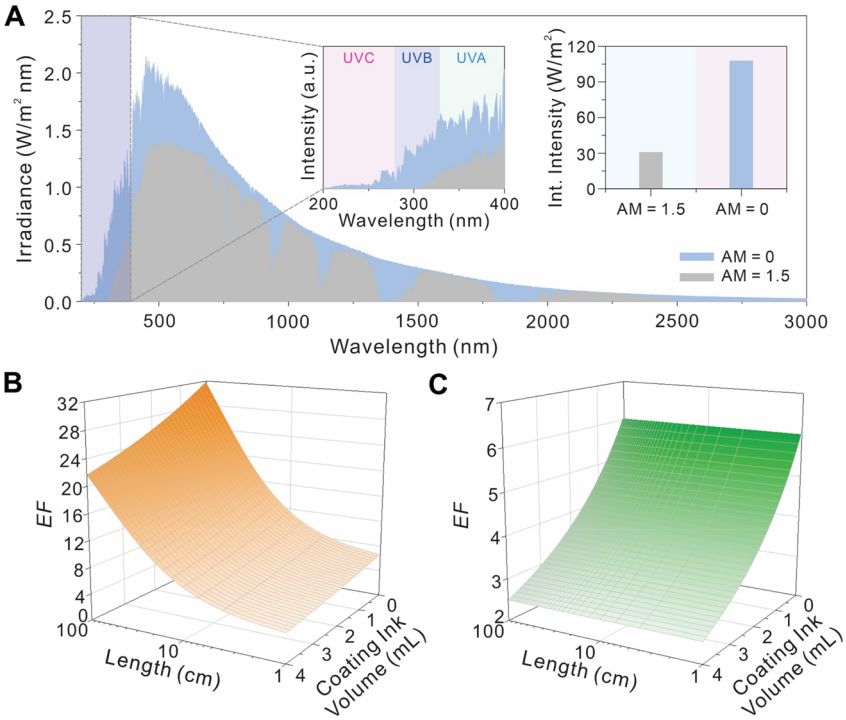

Figure 5. (A) Solar radiation spectra with AM = 0 (blue) and AM = 1.5 (gray). Insets: zoom-in spectra for the UV spectral region (left) and the integrated (Int.) solar radiation intensity in the UV wavelength range from 200 to 400 nm. (B, C) 3D plots of the enhancement factor (EF) evolutions as functions of the device length and the volume of the $Cs_3Cu_2Cl_5$ NDs coating ink solution for LSC (B) and LDS (C) devices.

the simulated solar illumination using a sunlight simulator (AM = 1.5), the short current density of the attached Si−PV cell showed a small increase from 16.4 mA/cm^2 (reference Si−PV), 16.5 mA/cm^2 (LDS-1-PV), 16.6 mA/cm^2 (LDS-2-PV), 16.8 mA/cm^2 (LDS-3-PV), 17.0 mA/cm^2 (LDS-4-PV) to 17.3 mA/cm^2 (LDS-5-PV) (Figure 4E). This limited short-current-density enhancement was mainly due to the small portion of UVB and UVC photons of the total solar spectrum (~0.05% of the total solar photons). However, when the LDS-PV systems were irradiated using a 305 nm UV light source, a maximum of 73% enhancement of the short-current-density can be obtained from 0.137 mA/cm^2 (reference standalone Si−PV), 0.163 mA/cm^2 (LDS-1-PV), 0.178 mA/cm^2 (LDS-2-PV), 0.195 mA/cm^2 (LDS-3-PV), 0.216 mA/cm^2 (LDS-4-PV) to 0.237 mA/cm^2 (LDS-5-PV) (Figure 4F). Taken together, our results unambiguously revealed that the $Cs_3Cu_2Cl_5$ NDs-based LSC or LDS photon-managing devices can greatly enhance the high-energy UV photon harvesting and power conversion through effective photon concentrating and/or energy down-shifting processes.

Finally, we explored the feasibility of implementing $Cs_3Cu_2Cl_5$ NDs-based photon-managing devices for the space-based solar power station through simulation studies. Figure 5A shows the comparison of solar spectra in space (AM = 0) and on earth (AM = 1.5). The integrated solar irradiation intensity for the UV portion (i.e., 200−400 nm) of the spectrum is ~3.5-fold increase in space as compared to that on the earth surface due to the strong UV absorption and scatting effects by the ozone (Figure 5A, insets).[17,18] In order to compare the LSC or LDS device performance in space and on earth, we simulated the device performances using incident solar spectra for both cases (see simulation details in the Supporting Information) and introduced an enhancement factor (EF), which is represented as follows:

$$\mathrm{EF} = \frac{\eta_{\mathrm{ext,AM=0}} - \eta_{\mathrm{ext,AM=1.5}}}{\eta_{\mathrm{ext,AM=1.5}}}$$

where $\eta_{\mathrm{ext,AM=0}}$ and $\eta_{\mathrm{ext,AM=1.5}}$ represent the external optical efficiencies of the device (applied as either LSC or LDS) under AM = 0 and AM = 1.5 solar radiation, respectively. As shown in Figure 5B, the EF for the LSC devices increased from 4.3 to 31.9 as increasing the length of the device (with a cuboidal geometry) from 1.0 to 100 cm or decreasing the volume of $Cs_3Cu_2Cl_5$ NDs coating ink solution from 4.0 to 0.04 mL. For the LDS device simulation, a universal enhancement in device performance with the EF > 2.4 was obtained regardless of the dimensions of the LDS device simulated in this study (Figure 5C). A maximal EF value of over 6.0 can be obtained when coating a thin layer of the $Cs_3Cu_2Cl_5$ NDs/PDMS film (coating solution volume of <0.1 mL) on the LDS device substrate. Taking together, our results proved that the $Cs_3Cu_2Cl_5$ NDs-based LSC/LDS devices are highly suitable for space-based solar power system applications and offer enhanced UV photon harvesting/utilization as compared to their conventional uses on earth.

We developed high-performance $Cs_3Cu_2Cl_5$ perovskite NDs-based photon-managing devices that can serve as LSC or LDS layers for PV cells. These perovskite NDs offer strong UV absorption, high PL QYs of >80%, and a large Stokes shift with reabsorption-free behaviors, making them ideal for high-energy UV photon harvesting and conversion in space-based solar power applications. The fabricated $Cs_3Cu_2Cl_5$ NDs/PDMS composite devices showed low photon scattering and high visible light transparency. Both experimental results and simulations demonstrated that when attached to Si−PV cells, the LSC or LDS devices outperformed standalone Si-PV systems for high-energy UV photon harvesting and power conversion. Our study suggests that using lead-free Cu-based

https://doi.org/10.1021/acs.nanolett.3c00641
Nano Lett. 2023, 23, 4367−4374

perovskite nanomaterials for energy harvesting in space is a promising direction to explore.

■ ASSOCIATED CONTENT

Supporting Information

The Supporting Information is available free of charge at https://pubs.acs.org/doi/10.1021/acs.nanolett.3c00641.

Synthesis method of $Cs_3Cu_2Cl_5$ perovskite NDs; method for the luminescent solar concentrator (LSC) and luminescent downshifting (LDS) layer fabrication, optical efficiency measurement, UV−vis absorption/transmission measurements, photoluminescence (PL), photoluminescence excitation (PLE), and PL quantum yield (PL QY) measurements, X-ray diffraction (XRD) measurements, current density−voltage (J−V) curve characterization, scanning electron microscopy (SEM) measurements and surface roughness measurements and transimission electron microscopy (TEM) measurements; method of factor mode simulation and Monte Carlo ray-tracing simulation; TEM images of the $Cs_3Cu_2Cl_5$ perovskite NDs; transmission spectrum of the $Cs_3Cu_2Cl_5$ NDs/PDMS composite; SEM images of $Cs_3Cu_2Cl_5$ NDs/PDMS composite film; absorption spectra of the $Cs_3Cu_2Cl_5$ NDs/PDMS composite devices; internal optical efficiency (η_{int}) for the $Cs_3Cu_2Cl_5$ NDs/PDMS composite LSC devices; external optical efficiency (η_{ext}) determined by different characterization methods and MC simulation results (PDF)

■ AUTHOR INFORMATION

Corresponding Author

Ou Chen − *Department of Chemistry, Brown University, Providence, Rhode Island 02912, United States;* orcid.org/0000-0003-0551-090X; Email: ouchen@brown.edu

Authors

Junyu Wang − *Department of Chemistry, Brown University, Providence, Rhode Island 02912, United States*

Tong Cai − *Department of Chemistry, Brown University, Providence, Rhode Island 02912, United States*

Complete contact information is available at: https://pubs.acs.org/10.1021/acs.nanolett.3c00641

Author Contributions

J.W. and O.C. conceived the overall idea. J.W. and T.C. performed the $Cs_3Cu_2Cl_5$ NDs syntheses and characterizations. T.C. conducted the XRD measurement. J.W. performed the MC ray-tracing simulations and analytical mode simulations. J.W. performed the SEM and TEM measurements and LSC and LDS device characterizations. J.W. and T.C. analyzed the data. J.W., T.C., and O.C. wrote the manuscript. O.C. supervised the entire project.

Notes

The authors declare no competing financial interest.

■ ACKNOWLEDGMENTS

O.C. acknowledges the support from Rhode Island NASA EPSCoR research infrastructure and development grant (80NSSC19M0045). SEM, TEM, and XRD measurements were performed at the Electron Microscopy Facility in the Institute for Molecular and Nanoscale Innovation (IMNI) at Brown University. J.W. thanks Zhenghong Dai and Nitin P. Padture for the help with optoelectronic devices measurements.

■ REFERENCES

(1) Kong, M.; Kang, C. H.; Alkhazragi, O.; Sun, X.; Guo, Y.; Sait, M.; Holguin-Lerma, J. A.; Ng, T. K.; Ooi, B. S. Survey of Energy-autonomous Solar Cell Receivers for Satellite−air−ground−ocean Optical Wireless Communication. *Prog. Quantum Electron.* **2020**, *74*, 100300.

(2) Rahman, M. M.; Selvaraj, J.; Rahim, N. A.; Hasanuzzaman, M. Global Modern Monitoring Systems for PV Based Power Generation: A Review. *Renew. Sust. Energ. Rev.* **2018**, *82*, 4142−4158.

(3) Ahmed, R.; Sreeram, V.; Mishra, Y.; Arif, M. D. A Review and Evaluation of the State-of-the-art in PV Solar Power Forecasting: Techniques and Optimization. *Renew. Sust. Energ. Rev.* **2020**, *124*, 109792.

(4) Jordan, D. C.; Kurtz, S. R. Photovoltaic Degradation Rates-an Analytical Review. *Progress in Photovoltaics: Research and Applications* **2013**, *21* (1), 12−29.

(5) Vernay, C.; Pitaval, S.; Blanc, P. Review of Satellite-based Surface Solar Irradiation Databases for the Engineering, the Financing and the Operating of Photovoltaic Systems. *Energy Procedia* **2014**, *57*, 1383−1391.

(6) Yang, Y.; Zhang, Y.; Duan, B.; Wang, D.; Li, X. Design Project for Space Solar Power Station (SSPS-OMEGA). *Acta Astronaut.* **2016**, *121*, 51−58.

(7) Li, W. Overview on Space Solar Power Station. *Adv. Astronaut. Sci. Technol.* **2022**, *5* (1), 1−2.

(8) Yermoldina, G. T.; Suimenbayev, B. T.; Sysoev, V. K.; Suimenbayeva, Z. B. Features of Space Solar Power Station Control System. *Acta Astronaut.* **2019**, *158*, 111−120.

(9) Glaser, P. E. Power From the Sun: Its Future. *Science* **1968**, *162* (3856), 857−61.

(10) Li, J.; Aierken, A.; Liu, Y.; Zhuang, Y.; Yang, X.; Mo, J. H.; Fan, R. K.; Chen, Q. Y.; Zhang, S. Y.; Huang, Y. M.; Zhang, Q. A Brief Review of High Efficiency III-V Solar Cells for Space Application. *Frontiers in Physics* **2021**, *8*, 631925.

(11) Sysoev, V. K.; Pichkhadze, K. M.; Feldman, L. I.; Arapov, E. A.; Luzyanin, A. S. Concept Development for a Space Solar Power Station. *Solar System Research* **2012**, *46* (7), 548−554.

(12) Meng, X.-L.; Xia, X.-L.; Sun, C.; Hou, X.-B. Adjustment, Error Analysis and Modular Strategy for Space Solar Power Station. *Energy Conversion and Management* **2014**, *85*, 292−301.

(13) Fan, G.; Duan, B.; Zhang, Y.; Li, X.; Ji, X. Full-spectrum Selective Thin Film Based Photonic Cooler for Solar Cells of Space Solar Power Station. *Acta Astronaut.* **2021**, *180*, 196−204.

(14) Fan, G.; Zhang, Y.; Ji, X.; Yang, Y. Two-Layer Ring Truss-Based Space Solar Power Station. *Energies* **2022**, *15* (8), 2936.

(15) Cable, T. L.; Sofie, S. W. A Symmetrical, Planar SOFC Design for NASA's High Specific Power Density Requirements. *J. Power Sources* **2007**, *174* (1), 221−227.

(16) Tu, Y.; Wu, J.; Xu, G.; Yang, X.; Cai, R.; Gong, Q.; Zhu, R.; Huang, W. Perovskite Solar Cells for Space Applications: Progress and Challenges. *Adv. Mater.* **2021**, *33* (21), 2006545.

(17) Fontenla, J. M.; Harder, J.; Livingston, W.; Snow, M.; Woods, T. High-resolution Solar Spectral Irradiance from Extreme Ultraviolet to Far Infrared. *J. Geophys. Res.* **2011**, *116*, 20108.

(18) Dobber, M.; Voors, R.; Dirksen, R.; Kleipool, Q.; Levelt, P. The High-Resolution Solar Reference Spectrum between 250 and 550 nm and Its Application to Measurements with the Ozone Monitoring Instrument. *Sol. Phys.* **2008**, *249* (2), 281−291.

(19) Meinardi, F.; Colombo, A.; Velizhanin, K. A.; Simonutti, R.; Lorenzon, M.; Beverina, L.; Viswanatha, R.; Klimov, V. I.; Brovelli, S. Large-area Luminescent Solar Concentrators Based on 'Stokes-shift-engineered' Nanocrystals in a Mass-polymerized PMMA Matrix. *Nat. Photonics* **2014**, *8* (5), 392−399.

(20) Wang, J.; Yuan, Y.; Schneider, J.; Zhou, W.; Zhu, H.; Cai, T.; Chen, O. Quantum Dot-based Luminescent Solar Concentrators Fabricated through the Ultrasonic Spray-Coating Method. *ACS Appl. Mater. Interfaces* **2022**, *14* (36), 41013−41021.
(21) Klimov, V. I.; Baker, T. A.; Lim, J.; Velizhanin, K. A.; McDaniel, H. Quality Factor of Luminescent Solar Concentrators and Practical Concentration Limits Attainable with Semiconductor Quantum Dots. *ACS Photonics* **2016**, *3* (6), 1138−1148.
(22) Zhou, Y.; Benetti, D.; Fan, Z.; Zhao, H.; Ma, D.; Govorov, A. O.; Vomiero, A.; Rosei, F. Near Infrared, Highly Efficient Luminescent Solar Concentrators. *Adv. Energy Mater.* **2016**, *6* (11), 1501913.
(23) Cai, T.; Wang, J.; Li, W.; Hills-Kimball, K.; Yang, H.; Nagaoka, Y.; Yuan, Y.; Zia, R.; Chen, O. Mn^{2+}/Yb^{3+} Codoped $CsPbCl_3$ Perovskite Nanocrystals with Triple-Wavelength Emission for Luminescent Solar Concentrators. *Adv. Sci.* **2020**, *7* (18), 2001317.
(24) Wang, J.; Yuan, Y.; Zhu, H.; Cai, T.; Fang, Y.; Chen, O. Three-dimensional Macroporous Photonic Crystal Enhanced Photon Collection for Quantum Dot-based Luminescent Solar Concentrator. *Nano Energy* **2020**, *67*, 104217.
(25) Kalytchuk, S.; Gupta, S.; Zhovtiuk, O.; Vaneski, A.; Kershaw, S. V.; Fu, H.; Fan, Z.; Kwok, E. C. H.; Wang, C.-F.; Teoh, W. Y.; Rogach, A. L. Semiconductor Nanocrystals as Luminescent Down-Shifting Layers To Enhance the Efficiency of Thin-Film CdTe/CdS and Crystalline Si Solar Cells. *J. Phys. Chem. C* **2014**, *118* (30), 16393−16400.
(26) Song, P.; Hase, S.; Zhao, S.; Xu, Z.; Iso, Y.; Isobe, T. Feasibility of Emission-Enhanced CsPbCl3 Quantum Dots Co-Doped with Mn^{2+} and Er^{3+} as Luminescent Downshifting Layers in Crystalline Silicon Solar Modules. *ACS Appl. Nano Mater.* **2022**, *5* (2), 2522−2531.
(27) Yang, D.; Liang, H.; Liu, Y.; Hou, M.; Kan, L.; Yang, Y.; Zang, Z. A Large-area Luminescent Downshifting Layer Containing an Eu^{3+} Complex for Crystalline Silicon Solar Cells. *Dalton Trans.* **2020**, *49* (15), 4725−4731.
(28) Geyer, S. M.; Scherer, J. M.; Moloto, N.; Jaworski, F. B.; Bawendi, M. G. Efficient Luminescent Down-shifting Detectors Based on Colloidal Quantum Dots for Dual-band Detection Applications. *ACS Nano* **2011**, *5* (7), 5566−71.
(29) Nakamura, Y.; Iso, Y.; Isobe, T. Bandgap-Tuned $CuInS_2$/ZnS Core/Shell Quantum Dots for a Luminescent Downshifting Layer in a Crystalline Silicon Solar Module. *ACS Appl. Nano Mater.* **2020**, *3* (4), 3417−3426.
(30) Phelan, M. E.; Needell, D. R.; Potter, M. M.; Bauser, H. C.; Ryczek, C. N.; Nuzzo, R. G.; Atwater, H. A. Photovoltaic Thermal Management in Luminescent Solar Concentrators. *2022 IEEE 49th Photovoltaics Specialists Conference (PVSC)* **2022**, 0820−0825.
(31) Brossard, M.; Hong, C.-Y.; Hung, M.; Yu, P.; Charlton, M. D. B.; Savvidis, P. G.; Lagoudakis, P. G. Novel Non-radiative Exciton Harvesting Scheme Yields a 15% Efficiency Improvement in High-Efficiency III-V Solar Cells. *Adv. Opt. Mater.* **2015**, *3* (2), 263−269.
(32) Zondag, S. D. A.; Masson, T. M.; Debije, M. G.; Noel, T. The Development of Luminescent Solar Concentrator-based Photo-microreactors: a Cheap Reactor Enabling Efficient Solar-powered Photochemistry. *Photochem. Photobiol. Sci.* **2022**, *21* (5), 705−717.
(33) Alexandre, M.; Chapa, M.; Haque, S.; Mendes, M. J.; Águas, H.; Fortunato, E.; Martins, R. Optimum Luminescent Down-Shifting Properties for High Efficiency and Stable Perovskite Solar Cells. *ACS Appl. Energy Mater.* **2019**, *2* (4), 2930−2938.
(34) Yang, J.; Bao, Q.; Shen, L.; Ding, L. Potential Applications for Perovskite Solar Cells in Space. *Nano Energy* **2020**, *76*, 105019.
(35) Kirmani, A. R.; Durant, B. K.; Grandidier, J.; Haegel, N. M.; Kelzenberg, M. D.; Lao, Y. M.; McGehee, M. D.; McMillon-Brown, L.; Ostrowski, D. P.; Peshek, T. J.; Rout, B.; Sellers, I. R.; Steger, M.; Walker, D.; Wilt, D. M.; VanSant, K. T.; Luther, J. M. Countdown to Perovskite Space Launch: Guidelines to Performing Relevant Radiation-Hardness Experiments. *Joule* **2022**, *6* (5), 1015−1031.
(36) Kirmani, A. R.; Ostrowski, D. P.; VanSant, K. T.; Byers, T. A.; Bramante, R. C.; Heinselman, K. N.; Tong, J.; Stevens, B.; Nemeth, W.; Zhu, K.; Sellers, I. R.; Rout, B.; Luther, J. M. Metal Oxide Barrier Layers for Terrestrial and Space Perovskite Photovoltaics. *Nat. Energy* **2023**, *8*, 191−202.
(37) Cai, T.; Dube, L.; Saghy, P.; Yang, H.; Chen, O. Progress in All-inorganic Heterometallic Halide Layered Double Perovskites. *Trends Chem.* **2023**, *5* (1), 29−44.
(38) Han, L. L.; Sun, B. B.; Guo, C.; Peng, G. Q.; Chen, H. Y.; Yang, Z.; Li, N.; Ci, Z. P.; Jin, Z. W. Photophysics in Zero-Dimensional Potassium-Doped Cesium Copper Chloride $Cs_3Cu_2Cl_5$ Nanosheets and Its Application for High-Performance Flexible X-Ray Detection. *Adv. Opt. Mater.* **2022**, *10* (6), 2102453.
(39) Liu, C.; Wang, L.; Fang, F.; Zhao, Z.; Pan, J.; Akram, J.; Shafie, S. B.; Talaighil, R. Z.; Li, Q.; Zhao, Z.; Wu, J.; Zhu, Z.; Lei, W.; Zhang, X.; Chen, J. Energy Down-Conversion $Cs_3Cu_2Cl_5$ Nanocrystals for Boosting the Efficiency of UV Photodetector. *Front. Mater.* **2021**, *8*, 682833.
(40) Zhao, S. Y.; Chen, C.; Cai, W. S.; Li, R.; Li, H. Y.; Jiang, S. Q.; Liu, M.; Zang, Z. G. Efficiently Luminescent and Stable Lead-free $Cs_3Cu_2Cl_5$@ Silica Nanocrystals for White Light-Emitting Diodes and Communication. *Adv. Opt. Mater.* **2021**, *9* (13), 2100307.
(41) Luo, Z.; Li, Q.; Zhang, L.; Wu, X.; Tan, L.; Zou, C.; Liu, Y.; Quan, Z. 0D $Cs_3Cu_2X_5$ (X = I, Br, and Cl) Nanocrystals: Colloidal Syntheses and Optical Properties. *Small* **2020**, *16* (3), 1905226.
(42) Li, Y.; Vashishtha, P.; Zhou, Z.; Li, Z.; Shivarudraiah, S. B.; Ma, C.; Liu, J.; Wong, K. S.; Su, H.; Halpert, J. E. Room Temperature Synthesis of Stable, Printable $Cs_3Cu_2X_5$ (X = I, Br/I, Br, Br/Cl, Cl) Colloidal Nanocrystals with Near-Unity Quantum Yield Green Emitters (X = Cl). *Chem. Mater.* **2020**, *32* (13), 5515−5524.
(43) Zhao, S.; Mo, Q.; Cai, W.; Wang, H.; Zang, Z. Inorganic Lead-free Cesium Copper Chlorine Nanocrystal for Highly Efficient and Stable Warm White Light-emitting Diodes. *Photonics Res.* **2021**, *9* (2), 187−192.
(44) Li, C.-X.; Cho, S.-B.; Kim, D.-H.; Park, I.-K. Monodisperse Lead-Free Perovskite $Cs_3Cu_2I_5$ Nanocrystals: Role of the Metal Halide Additive. *Chem. Mater.* **2022**, *34* (15), 6921−6932.
(45) Lian, L.; Zheng, M.; Zhang, P.; Zheng, Z.; Du, K.; Lei, W.; Gao, J.; Niu, G.; Zhang, D.; Zhai, T.; Jin, S.; Tang, J.; Zhang, X.; Zhang, J. Photophysics in $Cs_3Cu_2X_5$ (X = Cl, Br, or I): Highly Luminescent Self-Trapped Excitons from Local Structure Symmetrization. *Chem. Mater.* **2020**, *32* (8), 3462−3468.
(46) Zhou, Z.; Li, Y.; Xing, Z.; Sung, H. H. Y.; Williams, I. D.; Li, Z.; Wong, K. S.; Halpert, J. E. Rapid Synthesis of Bright, Shape-Controlled, Large Single Crystals of $Cs_3Cu_2X_5$for Phase Pure Single (X= Br, Cl) and Mixed Halides (X= Br/Cl) as the Blue and Green Components for Printable White Light-Emitting Devices. *Adv. Mater. Interfaces* **2021**, *8* (20), 2101471.
(47) Sumner, R.; Eiselt, S.; Kilburn, T. B.; Erickson, C.; Carlson, B.; Gamelin, D. R.; McDowall, S.; Patrick, D. L. Analysis of Optical Losses in High-Efficiency $CuInS_2$-Based Nanocrystal Luminescent Solar Concentrators: Balancing Absorption versus Scattering. *J. Phys. Chem. C* **2017**, *121* (6), 3252−3260.
(48) Li, H.; Wu, K.; Lim, J.; Song, H.-J.; Klimov, V. I. Doctor-blade Deposition of Quantum Dots onto Standard Window Glass for Low-loss Large-area Luminescent Solar Concentrators. *Nat. Energy* **2016**, *1* (12), 16157.

https://doi.org/10.1021/acs.nanolett.3c00641
Nano Lett. 2023, 23, 4367−4374